Astron. Astrophys. 319, 764–780 (1997)

ASTRONOMY
AND
ASTROPHYSICS

Measurement of mass distribution of galaxy clusters using the giant luminous arc statistics with Le Fèvre et al.'s arc survey data

M. Hattori[1,2], **K. Watanabe**[3], **and K. Yamashita**[4]

[1] Max-Planck-Institut für Extraterrestrische Physik (MPE), D-85740 Garching, Germany
[2] Astronomical Institute, Tôhoku University, Aoba Aramaki, Sendai 980, Japan
[3] National Astronomical Observatory Japan, 2-21-1 Osawa, Mitaka, Tokyo 181, Japan
[4] Information Processing Center, Chiba University, Chiba 263, Japan

Received 22 April 1995 / Accepted 20 April 1996

Abstract. We have constructed a scheme to predict the number of arcs that should be observed in clusters, that fully takes into account both the detection conditions in the arc survey and the evolution of the source galaxies. The scheme has been applied to Le Fèvre et al.'s arc survey data in order to constrain the models of cluster mass distribution. The canonical model of the source galaxy evolution proposed by Yoshii (1993) is adopted. We have found that any spherical cluster mass distribution models even with very small core radius, cannot reproduce a number of arcs as large as the number observed in Le Fèvre et al.'s arc survey. Recently, Bartelmann, Steinmetz & Weiss (1995; hereafter BSW) showed that their inhomogeneous model constructed numerically can produce a much larger number of giant luminous arcs than the non-singular isothermal sphere model with the same core radius and the same velocity dispersion as those in their model. However, we have found that their cluster mass distribution model cannot reproduce a number of arcs as large as observed. We suggest that one of the possible solutions to reproduce the observed arc number is that the clusters have inhomogeneities similar to these in BSW's model as a whole and that the core radius of the clusters may be much smaller than that in BSW's model. A speculation on the evolution of the cooling flow and the hot gas in the cluster central region is made based on this suggestion. A possible variation of the lens model with the non-thermal pressure is also briefly discussed in order to examine how it enhances the expected number of giant luminous arcs.

Key words: galaxies: clusters of – cosmology: gravitational lensing – X-rays: galaxies – cosmology: observations

1. Introduction

Soon after the first discovery of a giant luminous arc-like image in a distant cluster (Lynds & Petrosian 1986, Soucail et al. 1987), a redshift measurement of the giant luminous arc has proved that it is indeed a gravitationally distorted image of the distant background galaxy (Soucail et al. 1988). Many authors have been extensively developing the use of gravitational lens effects by clusters of galaxies as new cosmological tools to study the mass distribution in distant clusters of galaxies since this discovery (e.g., Nemiroff & Dekel 1989, Kaiser & Squires 1993, Wu & Hammer 1993, Miralda-Escudé & Babul 1995; for review, see Fort & Mellier 1994 and references therein). Miralda-Escudé & Babul (1995) and Wu (1994) compared the mass distributions in the clusters of galaxies determined by two different methods with each other, namely reconstruction of the mass distribution from observational data of (a) the giant luminous arcs and (b) the X-ray with an assumption of hydrostatic equilibrium, and they concluded that the estimated mass in the cluster by method (a) would be nearly a factor of 2 or 3 larger than that determined by method (b). The same discrepancy is recently reported for the most X-ray luminous cluster at $z = 0.451$ (Schindler et al. 1995 & 1996). However, it has been claimed that either the cluster mass distribution models or the models for the physical state of the gas in the cluster of galaxies used in these methods might be too simplified partially due to lack of detailed observational information of the clusters of galaxies and that this discrepancy could not be taken too seriously (Smail et al. 1995, Kneib et al. 1995, Waxman & Miralda-Escudé 1995).

Several authors have been discussing the use of not only the giant luminous arcs but also the so-called weak gravitational lens effects by the clusters of galaxies as possible tools of the reconstruction of the cluster mass distribution (Webster 1985; Tyson, Valdes & Wenk 1990; Kochanek 1990; Miralda-Escudé 1991; Kaiser & Squires 1993). This has the advantages that we can directly measure the convergence and shear fields in the clusters of galaxies without any ambiguity in the cluster mass distribution models and that the reconstruction of the mass distribution up to a large angular extent may be possible, although a lot of observational data with high angular resolution are required (Kaiser & Squires 1993). Several analyses based of this method have shown that the total mass derived from the gravitational lenses is 2 or 3 times larger than the mass derived from

Send offprint requests to: M. Hattori

the virial analyses (Fahlman et al. 1994; Carlberg, Yee & Ellingson 1994; Bonnet, Mellier & Fort 1994). However, this method may significantly suffer systematic errors, and a lot of efforts have been carried out to remove the systematic errors from the cluster-reconstruction algorithm (Schneider 1995; Kaiser et al. 1994; Schneider & Seitz 1995; Seitz & Schneider 1995; Bartelmann 1995). Recently, Squires et al. (1995) have reported that the total mass derived by both weak lensing and X-ray observations agreed within measurement errors. However, the mass reconstruction method based on weak lensing effects provides only a lower limit for the total mass of the cluster of galaxies.

Statistics of the giant luminous arcs has been recognized as a powerful tool to examine the mass distribution of the distant clusters (Miralda-Escudé 1993a, 1993b; Wu & Hammer 1993). Miralda-Escudé (1993a) has developed a formalism of the arc statistics with the elliptical lens models. Moreover, in order to examine a close comparison with the observational results, the effects of a finite seeing size and several source properties have been considered in detail (Miralda-Escudé 1993b). Wu & Hammer (1993) have shown that the capability of clusters to produce giant luminous arcs is very sensitive to the assumed gravitational mass distribution. They have concluded that the gravitational mass in the distant clusters should be much more centrally concentrated than the luminous matter to explain the high frequency of giant luminous arcs in distant clusters. Recently, the influence of asymmetry and substructure in the clusters on the arc statistics has been extensively studied by Bartelmann and his collaborators (Bartelmann & Weiss 1994; BSW; Bartelmann 1995). They have found that their numerically modeled clusters can produce more giant luminous arcs by a factor of two orders of magnitude than that of the spherically symmetric cluster models with the same degree of the central concentration and the same velocity dispersion as those in their model. They have concluded that the high rate of finding giant luminous arcs in the distant clusters (Le Fèvre et al. 1994) indicates a significant amount of asymmetry and substructures in the mass distribution of most distant clusters. All of the previous papers have shown that the arc statistics is a powerful tool to constrain the mass distribution in distant clusters.

Because of the potential importance and the potential power of these new methods, it is necessary to do more precise quantitative studies to constrain the mass distribution of the distant clusters with gravitational lensing. In this paper, we focus on the method based on the giant luminous arc statistics. Though we will adopt a similar method to that in Miralda-Escudé (1993a,b), we will use newly obtained data of the systematic arc survey by Le Fèvre et al.(1994) and more sophisticated treatment to do precise quantitative analysis. To see what we should improve, we summarize a standard procedure of studying the arc statistics. First of all, a systematic arc survey for a certain sample of distant clusters has to be done in order to compare the observed number of giant luminous arcs with the theoretical model prediction. Recently, Le Fèvre et al. (1994) have done the first systematic arc survey with a X-ray flux limited complete cluster sample. In this paper, we examine the arc statistics with their observational work. Secondly, theoretical model parameters should be categorized into known and unknown parameters. The known parameters for Le Fèvre et al. sample are X-ray properties (see Sect. 2.1), redshift of each cluster and the observational conditions when the arc survey has been done for each cluster. Although we have not yet obtained a direct observational results concerning the evolution of galaxies for a full range of the redshift up to the galaxy formation epoch, we can safely fix the galaxy evolution model to a canonical model (Bruzual & Kron 1980; Bruzual 1983; Arimoto & Yoshii 1986 & 1987) which can explain the chemical and spectral properties for various types of present-day galaxies with fundamental assumptions such as the star formation rate and the initial mass function for main sequence stars. It has also succeeded in explaining observed number count, color distributions and redshift distribution of faint galaxies (Tyson 1988; Yoshii & Takahara 1988; Fukugita et al. 1990; Yoshii & Peterson 1991; Yoshii 1993). The unknown parameters are properties of the cluster mass distributions. A cosmological density parameter, a cosmological constant and the Hubble parameter are also still unknown. However, we can ignore the dependence of the number of giant luminous arcs on these parameters since the dependence is much smaller than that on the cluster mass distributions (Wu & Hammer 1993; Sects. 3 and 5). Thirdly, conditions of the identification of giant luminous arcs have to be defined (see Sect. 2.4). Finally, theoretical predictions of number of the giant luminous arcs satisfying the required conditions in Le Fèvre at al. sample have to be examined for various models of the gravitational mass distribution with the fixed known parameters as those of Le Fèvre et al. By comparing the theoretically predicted number with the observed number, the cluster mass distribution models can be constrained. This is the most honest procedure to be carried out. However, most of the previous works could not succeed in fully following this procedure. Especially, the treatment of the detection conditions and the evolution of background galaxies has been mostly incomplete. Moreover, the precise cross comparison of the theoretical predictions with the observational arc survey data has not yet been done including Miralda-Escudé (1993b).

In this paper, the giant arc statistics is investigated by following the above mentioned way as possible as we can. The detection conditions and the luminosity evolution of the background galaxies are consistently taken into account in the theoretical framework, and we show a significant importance of the detection conditions in the study of arc statistics. The seeing smears surface brightness of the observed images (Yoshii 1993; Sect. 2.6) and smears out a fraction of high redshift faint galaxies below the limiting surface brightness (Yoshii 1993 for field galaxies; Miralda-Escudé 1993b & Sects. 3 and 5 for arcs). Therefore, any theoretical predictions without any considerations of the detection conditions leads overestimation of the number and wrong redshift distribution of the giant luminous arcs as shown in Sects. 3 and 5. A cross comparison of our model predictions with Le Fèvre et al.'s arc survey results (1994) is done, and the cluster mass distribution is then constrained.

2. Construction of Arc identification scheme

2.1. Theoretical model construction

As mentioned in the previous section, parameters are divided into known and unknown parameter groups. Firstly, properties of the known parameters are summarized. Redshifts of the clusters in Le Fèvre et al. (1994) sample are known parameters and summarized in Table 1. For simplicity, a spherically symmetric cluster hot gas and gravitational mass distribution model is assumed. The gas distribution in the nearby cluster is well approximated by the spherically symmetric form;

$$\rho_{\rm gas}(r) = \rho_{\rm gas}(0)\left[1+\left(\frac{r}{r_{\rm x}}\right)^2\right]^{-3\beta_{\rm x}/2}. \quad (1)$$

An average value of $r_{\rm x}$ for the distant EMSS clusters is $r_{\rm x} = 0.125h^{-1}$Mpc for non-cooling flow clusters and $r_{\rm x} = 0.1h^{-1}$Mpc for cooling flow clusters (Donahue, Stocke & Gioia 1992). An index, $\beta_{\rm x}$, for the best studied cluster Coma is 0.75 (Briel, Henry & Böhringer 1992), and this value can be also applied to the gas distribution in the nearby clusters well (Lubin & Bahcall 1993). We then assume that the gas distribution for all clusters in Le Fèvre et al. sample can be represented by Eq.(1) with $r_{\rm x} = 0.125h^{-1}$Mpc and $\beta_{\rm x} = 0.75$. The extent radius of the hot gas is assumed to be $1.5h^{-1}$Mpc. It might be oversimplification of the real cluster mass distribution. There is plenty of observational evidence indicating that a high fraction of the nearby clusters has significant amount of substructures and inhomogeneities (Jones & Forman 1990; Briel et al. 1991). We use a simple spherical mass distribution model in this paper for some technical reasons. However, as we will see, the study of arc statistics based on the simple spherical mass distribution models can still provide us insightful information. We can evaluate effects of the deviation of the cluster mass distribution from the spherical symmetry on the arc statistics with the present results as discussed in Sect. 5. Although the gas temperature of the most of distant clusters is still unknown, the gas temperature can be estimated in the following way with good accuracy. There is a good correlation between observed X-ray temperature and X-ray luminosity for the nearby clusters. David et al. (1993) has reported that fitting the data to a power-law relation, $kT_x = 10^a L_x^b$, gives $a = -0.59 \pm 0.02$ and $b = 0.290 \pm 0.004$, where kT_x is hot gas temperature in the unit of keV and L_x is 2-10keV luminosity in the unit of 10^{40}ergs s^{-1}. We assume that the above $T_x - L_x$ is also applicable to the distant clusters. Since X-ray photon counts rates by the Einstein observatory for Le Fèvre et al. sample are known, we estimate the best value of T_x for each cluster so as to reproduce the observed X-ray photon counts rate by keeping the $T_x - L_x$ relation. Metal abundance and a galactic absorption column density are assumed as $0.3Z_\odot$ and 10^{20}cm^{-2}, respectively, in this procedure. The results are summarized in Table 1.

The observational conditions in Le Fèvre et al. (1994) arc survey are as follows. The seeing FWHM was within the range from $0''.6$ to $1''.2$ with an average value $0''.8$. Hereafter, the average seeing FWHM is adopted as the seeing FWHM in the arc survey. The surface brightness limit for each observation is summarized in Table 1.

As will be discussed in Sect. 2.5, the intrinsic properties of galaxies including their evolution have been well quantified by the canonical model (Bruzual & Kron 1980; Bruzual 1983; Arimoto & Yoshii 1986, 1987; Yoshii & Takahara 1988; Yoshii 1993). This model has succeeded in explaining observed number count, color distribution and redshift distribution of faint galaxies. Variation of the evolutional models is limited by the chemical and spectral properties for various types of observed present-day galaxies (Arimoto & Yoshii 1986, 1987) and the number count of faint galaxies (Yoshii & Peterson 1991). We therefore fix the nature of the background galaxies according to this model.

The unknown parameters are those characterizing the mass distribution and the cosmological parameters. As we will see in Sect. 3, the arc statistics is insensitive to the background cosmology. Therefore, only the parameters in the cluster mass distribution model are effectively regarded as unknown parameters to be constrained by the arc statistics. We assume spherical mass distribution for the clusters;

$$\rho(r) = \begin{cases} \rho_{\rm c}\left[1+(r/r_{\rm c})^2\right]^{-3\beta_{\rm L}/2} & r \le R \\ 0 & r > R, \end{cases} \quad (2)$$

and we examine the cases of $\beta_{\rm L} = 2/3,\ 1$ and $4/3$. There are three free parameters, ρ_c, r_c and $\beta_{\rm L}$. By assuming a hydrostatic equilibrium for the gas distribution, number of the free parameters can be reduced to two, as will be explained in Sect. 2.2 in detail.

2.2. X-ray temperature and cluster mass distribution

Now, we decrease the number of the free parameters by the following procedure. A hydrostatic equilibrium in the adopted cluster mass distribution model is assumed. A temperature distribution in the hydrostatic gas is given by

$$T(r) = T_{\rm c}\left\{1-\chi\left(\frac{r_{\rm c}}{r_{\rm x}}\right)\int_0^y dy' \frac{1}{y'^2(1+y'^2)^{\frac{3}{2}\beta}} \times \int_0^{y'\frac{r_{\rm x}}{r_{\rm c}}} \frac{x^2}{(1+x^2)^{\frac{3}{2}\beta_{\rm L}}}dx\right\}(1+y^2)^{\frac{3}{2}\beta_{\rm x}}, \quad (3)$$

$$\chi = \frac{4\pi G\rho_{\rm c}r_{\rm c}^2}{\frac{k_{\rm B}T_{\rm c}}{\mu m_{\rm H}}}, \quad (4)$$

where $T_{\rm c}$ is central temperature of the hot gas and $y = r/r_{\rm x}$. Behavior of $T(r)$ is very sensitive to the assumed value of χ (Hughes 1989), and the temperature distribution is divided into two categories according to the condition whether χ is larger or less than the critical value defined by

$$\chi_{\rm cr} = \lim_{y\to\infty}\left\{\left(\frac{r_{\rm c}}{r_{\rm x}}\right)\int_0^y dy' \frac{1}{y'^2(1+y'^2)^{\frac{3}{2}\beta_{\rm x}}} \times \int_0^{y'\frac{r_{\rm x}}{r_{\rm c}}} \frac{x^2}{(1+x^2)^{\frac{3}{2}\beta_{\rm L}}}dx\right\}^{-1}. \quad (5)$$

Table 1. List of Le Fèvre et al. sample clusters

Cluster	z	T_x (keV)	S_V^L (mag/arcsec^2)	Cluster	z	T_x (keV)	S_V^L (mag/arcsec^2)
MS0015.9+1609	0.540	8	26.40	MS1333.3+1725	0.460	6	25.30
MS0302.7+1658	0.424	6	25.30	MS1358.4+6245	0.328	7	25.71
MS0353.6−3642	0.320	7	26.20	MS1455+2232	0.259	8	26.24
MS0451+0250	0.202	6	25.30	MS1512+3647	0.372	6	26.24
MS0735.6+7421	0.216	6	26.20	MS1621.5+2640	0.426	6	26.70
MS1006+1202	0.221	6	26.20	MS1910.5+6736	0.246	6	25.38
MS1008−1224	0.301	6	26.20	MS2053.7−0449	0.583	6	25.30
MS1224+2007	0.327	6	25.30	MS2137.3−2328	0.313	8	25.30

When χ is larger than $\chi_{\rm cr}$, the central gas pressure is not large enough to support the infinitely extended gas against the gravitational pull, and $T(r)$ gets a negative value at some finite radius. In the opposite case, the temperature is always positive, however, $T(r)$ increases rapidly from some finite radius, while the total pressure is kept almost constant. It means that the outer part of the gas distribution approaches to the pressure confined state. Since X-ray emitting regions of the most of the rich clusters extend, at least, up to $1.5h^{-1}$Mpc, and the gas temperature decreases at the cluster out skirt (Hughes 1989) rather than increases, only a narrow range of the values of χ around $\chi_{\rm cr}$ is acceptable to reproduce a realistic temperature distribution. Therefore, we assume that χ equals to $\chi_{\rm cr}$ and that the central temperature is given by $k_{\rm B}T_{\rm c}/\mu m_{\rm H} = 4\pi G\rho_{\rm c}r_{\rm c}^2/\chi_{\rm cr}$. Now a temperature profile has been fixed for each cluster gravitational mass distribution model. The extent of the X-ray emitting gas is assumed to be $r_{\rm ext} = 1.5h^{-1}$Mpc. We assume that the emission measure weighted X-ray temperature is the same as the observed temperature. The emission measure weighted X-ray temperature normalized by the central temperature, $T_{\rm c}$, is given by

$$T_{\rm em} = \frac{\int_0^{r_{\rm ext}} 4\pi r^2 n_e(r) n_i(r) \frac{T(r)}{T_{\rm c}} dr}{\int_0^{r_{\rm ext}} 4\pi r^2 n_e(r) n_i(r) dr}, \tag{6}$$

where n_e and n_i are electron number density and ion number density, respectively. Then we get a following relation which relates the cluster gravitational mass distribution models with the observed X-ray temperature,

$$4\pi G\rho_{\rm c}r_{\rm c}^2 = \chi_{\rm cr}\frac{1}{T_{\rm em}}\frac{k_{\rm B}T_{\rm obs}}{\mu m_{\rm H}}. \tag{7}$$

2.3. Cosmological gravitational lens theory

We summarize theoretical basis of the cosmological gravitational lens theory and some analytic results of our lens models in Appendix. A typical size of clusters of galaxies is $R \sim r_{\rm ext} = 1.5h^{-1}$Mpc, and when $\beta_L = 1$ or $4/3$ and $r_{\rm c} \leq r_{\rm x}$, we find that we can approximate the basic formulae in Appendix by those obtained by taking the limit, $R \to \infty$. However, when $\beta_L = 2/3$, we may overestimate the expected number of arcs, at most, by a factor of two if we use the formulae in the case of $R \to \infty$, and the difference becomes smaller as $r_{\rm c}/r_{\rm x}$ decreases. The lensing parameter, D, defined in Appendix is insensitive to the ambiguity of distance formulae namely the Dyer Roeder distance, and difference of the distance formulae is relevant with arc statistics only when $\Omega_0 \sim 1$ because both apparent magnitude and surface brightness decrease as $\tilde{\alpha}$ decreases. We numerically found that an ambiguity of the number of arcs induced by the ambiguity of the distance formulae in $\Omega_0 \sim 1$ models is, at most, factor of two when detection conditions are chosen as the same as those in Le Fèvre et al.'s arc survey.

It should be noted that, in deriving the basic formulae in Appendix, a source is assumed to have an infinitesimal size, and we should examine validity of this assumption. Let $\Sigma_L(\boldsymbol{\theta})$ and $\Sigma_0(\boldsymbol{\psi})$ be, respectively, surface brightness profiles of the source in the cases with and without gravitational lensing. An observed flux of the source with gravitational lensing is given by

$$f_L = \int \Sigma_L(\boldsymbol{\theta}) d\boldsymbol{\theta}, \tag{8}$$

where the integration about $\boldsymbol{\theta}$ is done within the region in which the surface brightness is larger than the observational threshold value. Since, as is shown from Ellis's reciprocal theorem (see e.g., Sasaki 1993), gravitational lens effects do not change the surface brightness:

$$\Sigma_0(\boldsymbol{\psi}) = \Sigma_L\left(\boldsymbol{\theta}[\boldsymbol{\psi}]\right), \tag{9}$$

the flux, f_L, is evaluated as

$$\begin{aligned} f_L &= \int \Sigma_0(\boldsymbol{\psi}) \left| \det\left(\frac{\partial\boldsymbol{\theta}}{\partial\boldsymbol{\psi}}\right)\right| d\boldsymbol{\psi} \\ &= \int A\left(\boldsymbol{\theta}[\boldsymbol{\psi}]\right) \Sigma_0(\boldsymbol{\psi}) d\boldsymbol{\psi}, \end{aligned} \tag{10}$$

where the image position vector, $\boldsymbol{\theta}$, and the integration region on the image plane are related with those on the source plane according to the lens equation. An infinitesimal source approximation assumes that the amplification factor, A, is approximately a constant function of the position within the image. That is, $f_L = A\ f_0$, where

$$f_0 = \int \Sigma_0(\boldsymbol{\psi}) d\boldsymbol{\psi}. \tag{11}$$

In other words, if the (unlensed) surface brightness weighted amplification factor, $< A > \equiv f_L/f_0$, can be approximated by

that for an infinitesimal source, A, we can safely use the basic formulae in Appendix. Note that the similar discussion can be applied to the axis ratio, ϵ.

Assuming the standard profile for the unlensed surface brightness (see Sect. 2.5), we numerically find that this approximation is valid when both of the following two conditions are satisfied: (a) a source size is smaller than $5h^{-1}$kpc, and (b) $A < 100$. When we choose the detection conditions as those in Le Fèvre et al.'s arc survey, we find that a surface brightness-limited size of M_B^* galaxies always satisfies the condition (a). As for the condition (b), even if the total magnitude of faint galaxies becomes brighter than the limiting magnitude of the arc survey, they could be hardly detected due to the surface brightness threshold in the arc survey. In conclusion, we may be able to neglect the finite size effects in analyzing Le Fèvre et al.'s data. However, it should be noted that it significantly depends on the adopted detection conditions whether the conditions (a) and (b) are satisfied and that one has to examine the validity of the infinitesimal source approximation when one analyzes other data of the arc survey under the different detection conditions. We use the basic formulae in Appendix in analyzing Le Fèvre et al.'s arc survey data.

2.4. Detection conditions and an arc identification scheme

For the purpose of illustrating effects of the detection conditions, we take a simplifying assumption that an image of the gravitationally lensed galaxy has an axially symmetric luminosity profile, $\tilde{g}(X, Y)$, which is convolved by a point-spread function, where X and Y stand for, respectively, the radius along the minor axis and the major axis of the lensed image in the unit of some scale, r_e. The integrated profile of $\tilde{g}(X, Y)$ up to an infinite radius is denoted by $\tilde{G}(\infty)$. The observed surface brightness at (X, Y) in X-band for the galaxy with absolute magnitude, M_X, is obtained as

$$\begin{aligned} S_X(X,\ Y)[\mathrm{mag/arcsec^2}] &= M_X + K_X + E_X \\ &+ 5\ \log[r_e(1+z_S)^2/10\mathrm{pc}] \\ &+ 26.5721 - 2.5\ \log[\tilde{g}(X,\ Y)/\tilde{G}(\infty)], \end{aligned} \tag{12}$$

where z_S is the redshift of the galaxy, and K_X and E_X are the K-correction and the evolutional correction in X-band, respectively. The limiting isophotal boundary, (X_p, Y_p), is determined by equating $S_X(X, Y)$ to the observational brightness threshold, S_X^L. For this image to be identified as a giant luminous arc, the axis ratio of the observed image has to be longer than some threshold value,

$$\text{axis ratio}\ \geq \epsilon_{\mathrm{th}}, \tag{13}$$

and, moreover, the diameter of the arc along the shortest axis has to exceed an imposed minimum value,

$$w_p > \frac{1}{2} D_{\mathrm{min}}, \tag{14}$$

where D_{min} is a seeing full width half maximum. Note that all giant luminous arcs identified by Le Fèvre et al. satisfy this condition.

The apparent isophotal magnitude, which is an apparent magnitude within the isophotal boundary (X_p, Y_p), is calculated by

$$\begin{aligned} m_X(S_X^L) = M_X + K_X + E_X + 5\ \log[D_S\ (1+z_S)^2/10\mathrm{pc}] \\ -2.5\ \log[\tilde{G}(S_X^L)/\tilde{G}(\infty)], \end{aligned} \tag{15}$$

where $\tilde{G}(S_X^L)$ is an integrated convolved luminosity profile within the isophotal boundary, (X_p, Y_p). The isophotal apparent magnitude has to be brighter than some threshold apparent magnitude for this image to be identified as a giant luminous arc,

$$m_X(S_X^L) \leq m_X(\mathrm{arc}). \tag{16}$$

We will also examine the expected arc numbers without the detection conditions to see how the detection conditions suppress the number of the detectable giant luminous arcs. In this case, 0-seeing FWHM, 0-minimum detectable radius and no surface brightness limit are assumed. Under these conditions, the giant luminous arcs are defined as an image, which has an axis ratio longer than the threshold value as described by Eq.(13) and has an apparent magnitude brighter than the threshold apparent magnitude as described by Eq.(16).

2.5. Intrinsic properties of galaxies

Prescriptions of the galaxy properties are essentially the same as those in Yoshii & Takahara (1988) and Yoshii & Peterson (1991). We classify galaxies into five morphological types. The type-mixing ratio given by Pence (1976) is adopted, that is (E/S0, Sab, Sbc, Scd, Sdm)=(0.215, 0.185, 0.160, 0.275, 0.165). The K and E corrections for each type are calculated by using the type-dependent, present day spectral energy distribution (SED) updated by Yoshii & Peterson (1991) and the type-dependent galaxy luminosity evolution models by Arimoto & Yoshii (1986, 1987), except for the UV light of E/S0 galaxies. We adopt both the UV-intermediate NGC 3379 SED and the UV-bright NGC 4649 SED as the SED of E/S0 galaxies. The galaxy formation epoch is assumed to be $z_F = 5$. The luminosity function of all galaxy types is assumed to be same and is taken from Efstathiou, Ellis & Peterson (1988), namely the Schechter function with $\alpha = -1.07$, $\phi_* = 1.56 \times 10^{-2} h^3 \mathrm{Mpc}^{-3}$ and $M_B^* = -19.39 + 5\log h$. The absolute magnitude in B band for each type of galaxies is converted into V band magnitude by $M_V = M_B + (V - B)$ where $(V - B) = 1.03$ for E/S0, 0.79 for Sab, 0.64 for Sbc, 0.56 for Scd and 0.46 for Sdm. No evolution for the galaxy luminosity function is assumed.

Following Yoshii (1993), a simple function with an integral index, n,

$$g(\beta) = \exp(-a_n \beta^{1/n}) \text{ with } \beta \equiv r/r_e, \tag{17}$$

is used to represent the $1/4$ law profile for elliptical galaxies as well as the bulge component of spiral galaxies ($n = 4$, $a_4 = 7.67$; de Vaucouleurs 1962) and the exponential profile for the disk component of spiral galaxies ($n = 1$, $a_1 = 1.68$; Freeman 1970). In the following discussion, we simply assume the exponential

profile to all the spiral galaxy types since contribution of the bulge component to the total luminosity of spiral galaxies is very small (Yoshii 1993). As we will see in Sect. 7, the contribution of the bulge component does not change the model prediction of the total arc number significantly. The effective radius of a galaxy, r_e, is related to its absolute magnitude by

$$-M_{B_J}(\mathrm{mag}) = p \log r_e(\mathrm{kpc}) + q + (p-5)\log(h/0.5), \quad (18)$$

where p and q are defined as $p = 5$ and $q = 15.79$ for the disk galaxies (Freeman 1970) and $p = 3.3$ and $q = 18.43$ when $M_{B_J} < -18.5 + 5.0\log h$, and $p = 10$ and $q = 14.29$ when $M_{B_J} > -18.5+5.0\log h$ for E/S0 galaxies (Binggeli, Tarenghi & Sandage 1990).

2.6. Smeared luminosity profiles of the lensed images

Smeared luminosity profiles of the lensed images are modeled by the following way. Suppose that every points in the unlensed image of the source, $(x,\ y)$, are mapped into $x' = A_1 x$ and $y' = A_2 y$, where a coordinate of the center of the image is chosen as $(0, 0)$, and A_1 and A_2 are assumed to be constant within the image of the source. The unit of the scale is r_e. Since the surface brightness of the image is conserved by the gravitational lens effect, the luminosity profile of the lensed image, $g'(x',\ y')$, is related to the luminosity profile of the unlensed image by

$$g'(x',\ y') = g(\beta), \quad \text{where} \quad \beta = \sqrt{\left(\frac{x'}{A_1}\right)^2 + \left(\frac{y'}{A_2}\right)^2}. \quad (19)$$

Taking a Gaussian point-spread function with dispersion σ_t on the source plane, the smeared luminosity profile has the form,

$$\tilde{g}(X,\ Y) = \int g\left[\sqrt{\left(\frac{x'}{A_1}\right)^2 + \left(\frac{y'}{A_2}\right)^2}\right] \times \frac{1}{2\pi\sigma_t^2}\exp\left[-\frac{1}{2\sigma_t^2}\left\{(x'-X)^2 + (y'-Y)^2\right\}\right] dx'\ dy'. \quad (20)$$

The seeing FWHM on the image plane is referred back to the dispersion, σ_t, on the source plane by

$$\text{seeing FWHM} = 2\sqrt{2\ln 2}(r_e/D_S)\sigma_t. \quad (21)$$

We show in Fig. 1 the smeared $1/4$ law profile and the exponential luminosity profiles along the longest axis and the shortest axis of the source galaxies with $M_* + 5$, where seeing FWHM=0″.8, $z_S = 1$ and $(\Omega_0,\ \lambda_0,\ h) = (1, 0, 0.5)$. In general, the surface brightness of the smeared image is brighter for the larger image deformation rate since the relative scale of the seeing FWHM to the magnified image becomes smaller. Therefore, more distant galaxies are observable through the lensing cluster than the case without any lensing cluster in the field of view. When we fix A_1, the brightening of the surface brightness is stopped at the certain value of A_2 before reaching the intrinsic surface brightness of the source. To recover the intrinsic surface brightness, A_1 must have a larger value as A_2 is getting larger.

2.7. Numerical methods

We numerically calculate a cross-section for a cluster of galaxies to make giant luminous arcs of the background galaxies in the following way. There are two critical lines on the lens plane where the amplification factor becomes infinity. We numerically search four boundaries around the critical lines on the lens plane, where the boundaries define two distinct regions according to the condition whether the required conditions for giant luminous arcs are satisfied or not. This procedure is done for all different types of background galaxies in the magnitude range from $M_B^* - 5$ to $M_B^* + 8$ with a magnitude interval, 0.2. The redshift range is taken from $z_S = z_{cr}$ to $z_S = z_F$ with a redshift interval, 0.01, where z_{cr} is the redshift at which the lensing parameter, D, becomes the critical value. These boundaries on the lens plane are transformed into the boundaries on the source plane by the lens equation in order to obtain the cross-section on the source plane.

Detailed numerical methods of searching of the boundaries are different between the cases of with and without the detection conditions. In the case without the detection conditions, we first search the boundaries on which the axis ratio of the image equals to the threshold value. Next, an apparent magnitude of the lensed image is calculated on each boundary. If the apparent magnitude is brighter than the threshold value, the present boundary is regarded as a boundary of the forming region of the giant luminous arcs. If the apparent magnitude is fainter than the threshold value, we search another boundary on which the apparent magnitude equals to the threshold value, and this new boundary is regarded as a boundary of the forming region of the giant luminous arcs. The numerical procedure is done by the Newton-Raphson method with very high accuracy. To prevent missing the boundary, an initial stage of each boundary search is done by the Newton-Raphson method with deceleration. To check the accuracy of the boundary search procedure, parity, axis ratio and magnitude of the image on the boundary are examined.

Next, the procedure in the case with the detection conditions is summarized. Main differences from the case without the detection conditions are that we have to first calculate a surface brightness profile of the smeared images by the finite seeing and then search a limiting isophotal boundary in the image. It is practically impossible to exactly take into account a surface brightness profile of the smeared images in calculating the cross-section. Instead, we are using a numerical table of $\tilde{g}(0, Y)$ in 3 dimensional space $(\sigma_t/A_1, \sigma_t/A_2, Y)$ for the $1/4$ law profile and the exponential profile in order to calculate the smeared surface brightness profile along major and minor axes. When the surface brightness profile of the smeared image is calculated for an arbitrary combination of σ_t/A_1 and σ_t/A_2 using the numerical table with a finite grid size of $(\sigma_t/A_1, \sigma_t/A_2)$, values on the neighboring four grid points are averaged by the same rule as a cloud in cell method. The major and minor axes are then found by using the approximated surface brightness profile of the smeared image calculated by the above procedure. The apparent magnitude of seeing smeared, surface brightness limited,

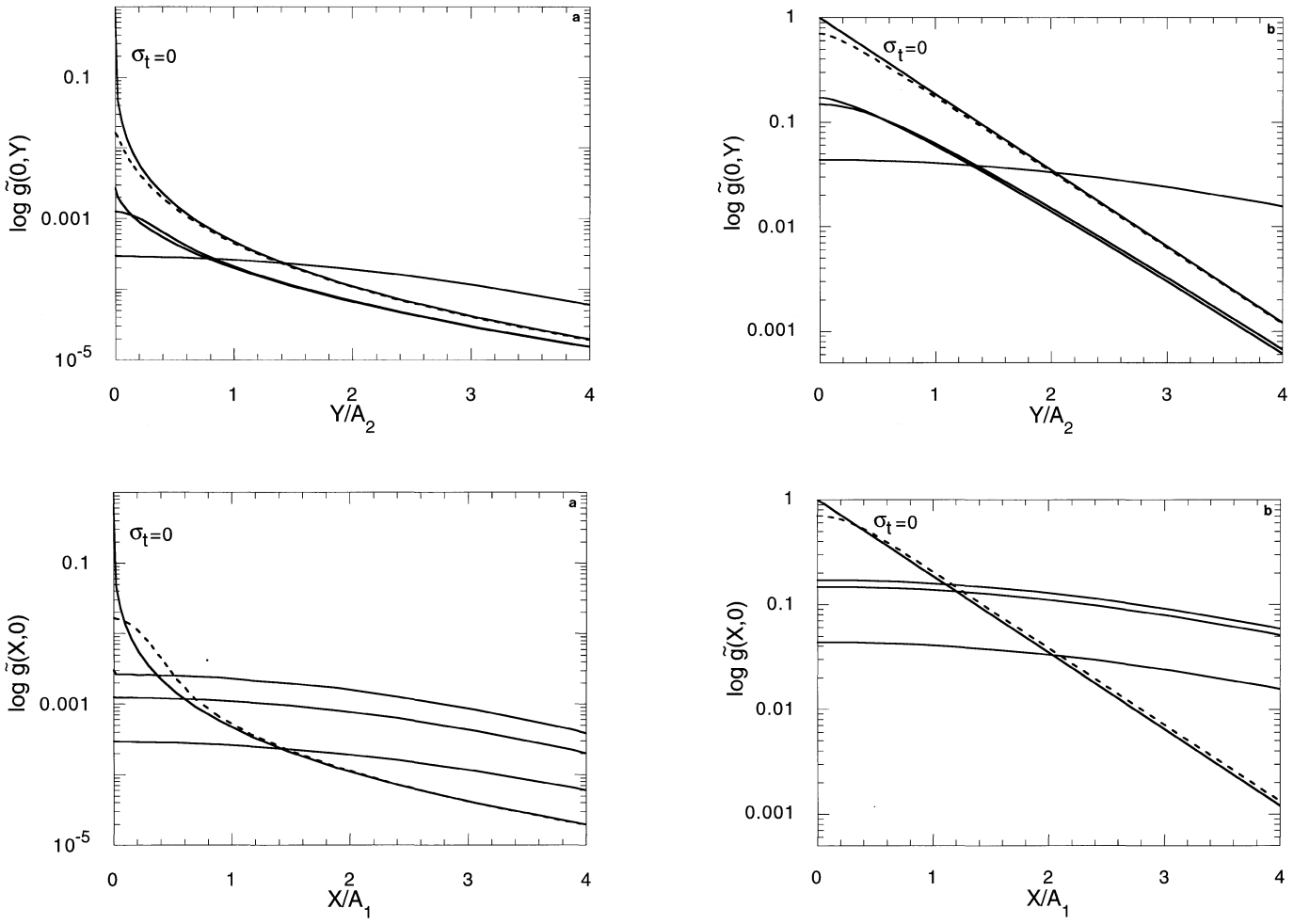

Fig. 1a and b. Effects of amplification on the surface brightness distribution for an image of the lensed galaxy with **a** the $1/4$ law profile and **b** the exponential profile. The units of the horizontal axes is the effective radius of the galaxy in the image plane, that is $A_1 \times r_e$ for minor axis and $A_2 \times r_e$ for major axis. We assume that $M = M_* + 5$, $z_S = 1$, and $(\Omega_0, \lambda_0, h) = (1.0, 0.0, 0.5)$. The lines denoted by $\sigma_t = 0$ show the intrinsic surface brightness distribution of the source galaxies. The upper panel shows the smeared surface brightness along the major axis for $(A_1, A_2) = (1, 1),\ (1, 10),\ (1, 1000)$ (solid lines from bottom to top at the left side of the figures) and (10,100) (dashed lines). The lower panel shows the smeared surface brightness along the minor axis for the same combinations of (A_1, A_2) as the upper panel.

lensed image is approximately calculated by

$$m_X(S_X^L) \sim M_X + K_X + E_X + 5\,\log[D_S\,(1+z_S)^2/10\mathrm{pc}] \\ -2.5\,\log\left[A_1 A_2 G\left(\frac{\ell_p}{2A_2}\right)/G(\infty)\right], \qquad (22)$$

where ℓ_p is a diameter of the surface brightness limited image along the major axis in the unit of r_e, A_2 is an image deformation rate along major axis and G is an integrated intrinsic luminosity profile. We have made sure how accurate this approximation is by comparing the results obtained by the above approximated procedure with the results obtained by direct calculations, that is, dividing an image into precise grid points, calculating the smeared surface brightness on each grid point and calculating the apparent magnitude within the limiting isophotal boundary. The agreement between both results are very well for $\ell_p > 2\times$ seeing FWHM. Since we are interested in the arcs with a length several times longer than the seeing FWHM, we can safely apply this approximation to our following investigations. The boundary search procedure is as follows. First, the boundaries on the lens plane on which axis ratio of the unsmeared image equals to the threshold value are searched by the Newton-Raphson method. Since the axis ratio of the smeared image is generally smaller than that of the unsmeared image due to stronger smearing along the shortest axis, Eq.(13) is not satisfied on these boundaries found in the unsmeared image. We therefore start to look for correct boundaries by increasing the threshold value of the axis ratio little by little from $\epsilon_{\rm th}$ until all three conditions, Eqs.(13), (14) and (16) are satisfied. To test validity of this numerical code, the results obtained by this method in the case of a small seeing FWHM and an extremely faint surface brightness limit are compared with the results ob-

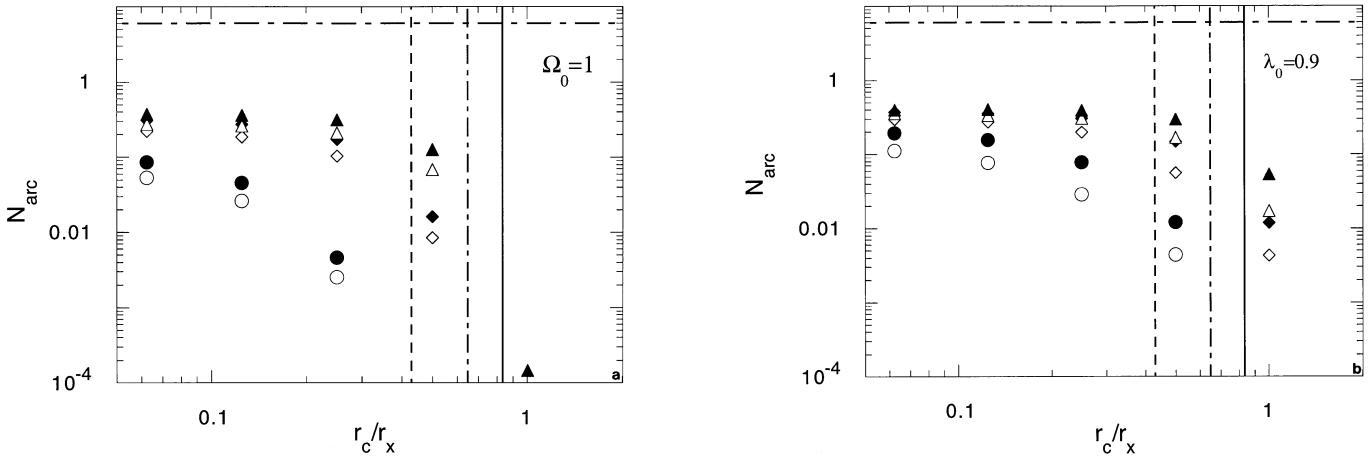

Fig. 2a and b. Model predictions of the number of the giant luminous arcs in Le Fèvre et al. (1994) sample in **a** $(\Omega_0, \lambda_0, h) = (1.0, 0.0, 0.5)$ universe and **b** $(\Omega_0, \lambda_0, h) = (0.1, 0.9, 1.0)$ universe. All of the detection conditions are taken into account. The predicted arc number is shown as a function of r_c/r_x for $\beta_L = 2/3$ (circle), 1 (diamond) and $4/3$ (triangle). Open and filled symbols correspond to the results with NGC 3379 SED and with NGC 4649 SED, respectively. A horizontal short dashed line shows the number of the giant luminous arcs found in Le Fèvre et al. sample. Three vertical lines show the critical core radius where the ICM distribution is marginally unstable against the convective instability for $\beta_L = 2/3$ (dashed line), $\beta_L = 1$ (dashed-dotted line) and $\beta_L = 4/3$ (solid line). When the core radius of the cluster mass distribution is less than the critical value, a convectively unstable region appears in the central part of the ICM.

tained in the case without the detection conditions. We have got a good agreement between both results.

3. Arc statistics I

Now we are ready for investigating the model prediction of number of the giant luminous arcs in Le Fèvre et al. sample. The threshold values of the axis ratio, the minimum diameter of the shortest axis and the threshold apparent V magnitude are set to be $\epsilon_{\rm th} = 10$, $D_{\rm min} = 0''.8$ and $m_V({\rm arc}) = 22.5$, respectively. Le Fèvre et al. (1994) has found 6 arcs satisfying these conditions in the field of their sample clusters. Observational conditions summarized in Sect. 2.1 are taken into account. The expected number of giant luminous arcs in Le Fèvre et al. sample under these conditions, $N_{\rm arc}$, is calculated by summing up all the expected number of the arcs in each cluster, $N_{i,{\rm arc}}$,

$$N_{i,{\rm arc}} = \frac{c}{H_0} \sum_{{\rm X_{type}=E/S0}}^{\rm Sdm} \int_0^{z_F} dz_S \times \frac{(1+z_S)^2}{\sqrt{\Omega_0(1+z_S)^3 + (1-\Omega_0-\lambda_0)(1+z_S)^2 + \lambda_0}} \times \int_{L_B(M_B^*+8)}^{L_B(M_B^*-5)} \frac{dL_B}{L_B^*} \phi(L_B, {\rm X_{type}}) \times \sigma_i((\ell/w)_p \geq \epsilon_{\rm th}, m_V(S_V^L) \leq m_V({\rm arc}), w_p > D_{\rm min}/2 : L_B, z_S, {\rm X_{type}}), \quad (23)$$

where i is the number specifying the cluster in Le Fèvre et al. sample and is in the range from 1 to 16, $L_B(M_B^* + 8)$, L_B^* and $L_B(M_B^* - 5)$ are present blue luminosity of galaxies with absolute blue magnitude M_B^*+8,M_B^* and M_B^*-5, respectively, $\phi(L_B, {\rm X_{type}})$ is the present luminosity function of galaxies of type $\rm X_{type}$, and $\sigma_i((\ell/w)_p \geq \epsilon_{\rm th}, m_V(S_V^L) \leq m_V({\rm arc}), w_p > D_{\rm min}/2 : L_B, z_S, {\rm X_{type}})$ is the cross-section for a cluster i to make giant luminous arcs of the background galaxy of type $\rm X_{type}$ with present blue luminosity L_B at redshift z_S. Note that the cross-section is always zero for $z_S < z_{cr}$.

In Fig. 2 we show the predicted number of the giant luminous arcs in Le Fèvre et al. sample as a function of the core radius in the cluster mass distribution model. The results are shown for $\beta_L = 4/3$ (triangles), 1 (diamonds) and $2/3$ (circles) in $(\Omega_0, \lambda_0, h) = (1.0, 0, 0.5)$ and in $(0.1, 0.9, 1.0)$ universes. First of all, no model can explain the observed large number of the giant luminous arcs in Le Fèvre et al. sample. All model predictions are much less than the observed number. There is a general tendency that the expected number of the giant luminous arcs is larger for the more centrally concentrated mass distribution models, that is, for a larger β_L or for a smaller r_c. A more central concentration of the cluster mass distribution than the X-ray emitting gas distribution is favorable to reproduce the observed high frequency of finding giant luminous arcs although the predicted number in the limiting case, $r_c \to 0$, is still less than the observed number of the arcs. The expected number is saturated at some value of r_c. We cannot expect further increase of the predicted number with further decrease of the core radius. An effect of the cosmological parameters, (Ω_0, λ_0), in the predicted number is very small compared with its sensitive dependence on the mass distribution model, as shown by Wu & Hammer (1993). Open and filled symbols are corresponding to the results with NGC 3379 SED and with NGC 4649 SED, respectively. The difference of the results between the NGC 3379 and NGC 4649 SED model predictions are small, and the NGC 4649 SED model predic-

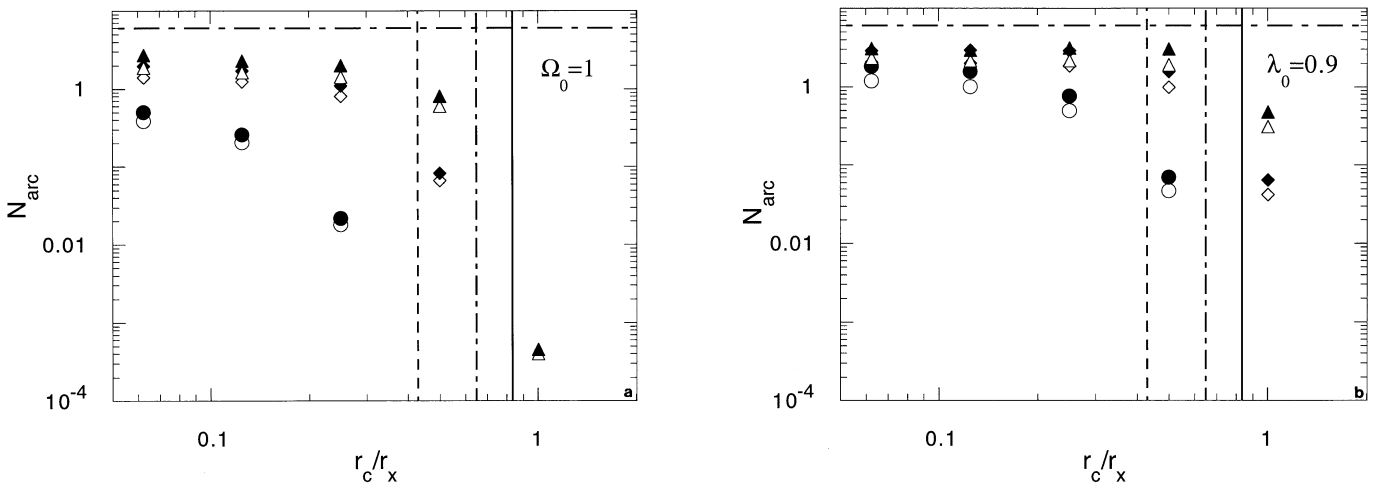

Fig. 3a and b. Predicted number of the giant luminous arcs in the case without any detection conditions in **a** $(\Omega_0, \lambda_0, h) = (1.0, 0.0, 0.5)$ universe and **b** $(\Omega_0, \lambda_0, h) = (0.1, 0.9, 1.0)$ universe. Meaning of the symbols and lines are the same as those in Fig. 2.

tions are always slightly larger than the NGC 3379 SED model predictions. In Fig. 3 we show the model predictions when all detection conditions are negligible. We have found that inclusion of the detection conditions significantly decreases number of the detectable giant luminous arcs. In Fig. 4 the distribution of the number of the arcs against the source size is shown. It shows that the most of the arcs are made from the source galaxies with r_e ∼seeingFWHM. The number of the arcs made by the source galaxies with r_e ∼seeingFWHM is maximum. A drastic decrease of the arc number below the galaxy size of seeingFWHM is consistent with the results shown by Miralda-Escudé (1993b). The gradual decrease of the arc number made from the larger size galaxy could be due to the rapid decrease of the number density of bright, namely large r_e, galaxies.

Although we have assumed circular symmetric shape for all the source galaxies, intrinsic elongation of the source galaxies, especially spiral galaxies, could increase the expected number of giant luminous arcs. We will roughly estimate how the intrinsic shape effects affect the expected number of the giant luminous arcs. For simplicity, let us assume that a spiral galaxy is a thin disk with a homogeneous surface brightness distribution. If we neglect the dust obscuration in the spirals, the luminosity-weighted intrinsic shape is $\epsilon_{\rm int} \sim \pi/2 \sim 1.6$, and the threshold value, $\epsilon_{\rm th}$, is deduced by a factor, $1/\epsilon_{\rm int}$. An average of the optical depth of the dust obscuration is still uncertain (e.g. Heisler & Ostriker 1988).

However, some spirals may be significantly optically thick as NGC 3314 whose optical depth is larger than 1.4 (James & Puxley 1993). For comparison, we examine the expected number of giant luminous arcs with the reduced value of $\epsilon_{\rm th}$. The reduced value of $\epsilon_{\rm th}$ increases the expected number of giant luminous arcs by a factor of two. However, it is still too small to explain the observed number of giant luminous arcs in the Le Fèvre et al. sample.

The possibility of higher number density and brighter luminosity of the background galaxies than the presently adopted model could increase the predicted number of the giant luminous arcs. However, the evolutional nature of the background galaxies should be consistent with the observed number count, color distributions and redshift distribution of faint galaxies. For example, from the color distributions, Yoshii & Peterson (1993) have concluded that a redshift of the epoch of galaxy formation must be greater than three. We have confirmed that the results are insensitive even if the galaxy formation epoch is set to be the latest possible one, that is $z = 3$. Recently, several deep surveys are trying to examine the nature of high redshift galaxies (e.g. Griffiths et al. 1994; Crampton et al. 1994). These works will fix the ambiguities in the evolutional history of galaxies and help us to reduce uncertainty in the constrained cluster mass distribution models by the arc statistics.

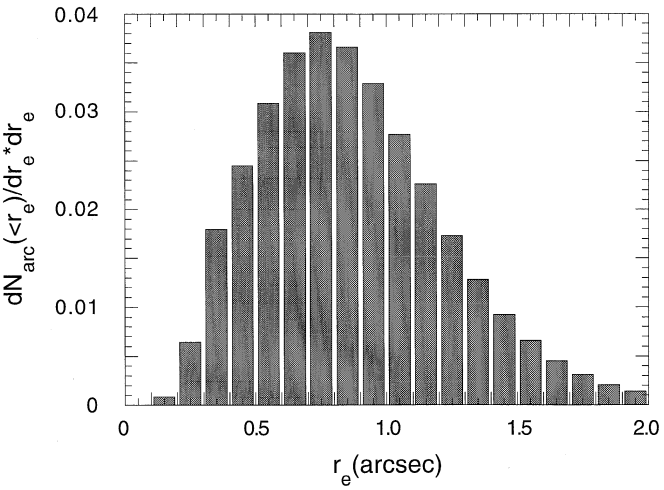

Fig. 4. The distribution of the giant luminous arc number against the intrinsic size of source galaxies. The results are shown for $(\Omega_0, \lambda_0, h) = (0.1, 0.9, 1.0)$ universe and NGC 3379 SED case. The last histogram is number of arcs in the range of $r_e > 1''.9$.

4. A roll of inhomogeneities in the arc statistics

We have assumed a spherical lens model. However, as is shown with the geodesic deviation equation (e.g. Hawking & Ellis 1973), inhomogeneities in the clusters of galaxies, (e.g., presence of cD galaxies and substructures, deviation of the cluster shape from spherical symmetry) may increase the capability of clusters to produce the giant luminous arcs (Miralda-Escudé 1993a; Bartelmann & Weiss 1994; BSW; Bartelmann 1995). We investigate whether the inhomogeneities in the cluster mass distribution can solve the arc deficiency problem on the basis of BSW's work. Bartelmann, Steinmetz & Weiss (BSW) have pointed out that the capability of their numerically modeled clusters to produce giant luminous arcs is larger by two order of magnitude than that of spherically symmetric cluster mass distribution models with the same core radii and velocity dispersions as those in their model. However, it is unlikely that their numerical modeled clusters can reproduce the observed number of giant luminous arcs in Le Fèvre et al. sample. First of all, their non-singular isothermal sphere model compared with the numerical model has a relatively large core radius, that is $r_{\rm c}/r_{\rm x} \sim 80{\rm kpc}/130{\rm kpc} \sim 0.6$, while we have shown that a cluster with a much smaller core radius than this value has the more than two order of magnitude larger capability to produce the giant luminous arcs than that of the cluster with the same core radius as BSW. Since the cluster with a much smaller core radius still could not reproduce the observed number in Le Fèvre et al. sample, it is unlikely that the BSW's numerically modeled cluster can explain the observations. Now, we show the situation quantitatively. They have shown that the capability of the singular isothermal sphere model with the same velocity dispersion is almost same as and even slightly larger than that of their model cluster. The singular isothermal sphere model is identical to our model with $\beta_{\rm L} = 2/3$ in the limit of $r_{\rm c} \to 0$. As shown in Sect. 3 and 4, the predicted number in the singular isothermal model is still much smaller than the observed number when the detection conditions are fully taken into account. Therefore, we conclude that BSW's numerically modeled cluster could not reproduce the high frequency of detecting the giant luminous arcs in Le Fèvre et al. sample.

In spite of the fact mentioned above, inhomogeneities in the cluster mass distribution could play an important role in the arc statistics. Firstly, since the direct observational evidence of highly asymmetric and substructural features of the clusters is drastically increasing (Jones & Forman 1990; Briel et al. 1991; Briel, Henry & Böhringer 1992), it is very natural to assume that the Le Fèvre et al. sample clusters are also suffering significant deviation from the spherical symmetry. Secondly, the nature of mass distribution in the central region of BSW's model clusters could be significantly affected by numerical resolution and lack of the gas dynamical process in their simulation. The core radius of their numerically modeled clusters, $80 \pm 20h^{-1}$kpc, is only $2-3$ times larger than the softening radius, $25h^{-1}$kpc. It is likely that the scale length of the core radius is limited by the numerical resolution. In addition, although they neglected gas dynamical effects on the formation of the cluster, there is a plenty of observational evidence indicating that a significant fraction of the mass in the central part of the cluster could be made by the gas-cooling process, namely the mass deposition process due to thermal instability in cooling flows (Fabian 1994; Hattori, Yoshida & Habe 1995). The modeling of the mass distribution based on the simulation without gas dynamics could lead underestimation of the mass in the central region of the cluster. More realistic numerical simulations of cluster formation with higher resolution and with gas dynamics are required. We support, for these two reasons, the idea that the mass concentration in the clusters of galaxies is much higher than that in BSW's numerically modeled clusters, even though they have inhomogeneities similar to that in BSW's model clusters as a whole. This improved cluster model could predict giant luminous arcs more than that of both spherical symmetric cluster model and BSW's numerical model. It is worth while examining the arc statistics on the basis of the improved cluster mass distribution models quantitatively. We are planning to examine the arc statistics based on the cluster mass distribution models with quantifying the asymmetry and inhomogeneity of the mass distribution using the ROSAT HRI images for each sample cluster.

5. Convectively unstable core and speculation on the evolution of the cooling flows

As discussed in previous section, one of the possibilities to reproduce the observed number of giant luminous arcs in Le Fèvre et al. sample is that the mass distribution in the distant clusters might have a large inhomogeneity and a high central concentration. This has an important suggestion on the evolution of the ICM.

Before we give speculation on the evolution of the ICM, we show that the presently adopted gas density distribution which is a good representative of the gas distribution in the nearby non-cooling flow clusters like Coma cluster, is convectively unstable if the core radius of the cluster mass distribution is more than 2 times smaller than the core radius of the gas density distribution. We show distributions of temperature and specific entropy in the small core radius model, $r_{\rm c} = r_{\rm x}/8$ in Fig. 5 for each value of $\beta_{\rm L}$. A negative entropy gradient region, in another word, a convectively unstable region, appears in the central part of the cluster. The e-fold time of the growth of the convective instability (e.g. Defouw 1970) is given by

$$t_{\rm conv} = \left(\sqrt{-g \left(\frac{T_{\rm c}}{T} \right) \frac{1}{\gamma} \left(\frac{\rho}{\rho_{\rm c}} \right)^{\gamma-1} \frac{d\, s}{d\, r}} \right)^{-1}, \qquad (24)$$

where $\gamma = 5/3$ is an adiabatic index, g is a cluster gravitational acceleration, s is a specific entropy normalized by the central value as $s = (P/\rho_{\rm gas}^{\gamma})/(P_{\rm c}/\rho_{\rm gas}(0)^{\gamma})$, P, T and $\rho_{\rm gas}$ are a gas pressure, gas temperature and gas density distribution, respectively. The time scale, $t_{\rm conv}$, within the convectively unstable region for $r_c/r_x = 1/8$ and $T_x = 8$keV is shown as a function of r in Fig. 6. It shows that the convective mixing time is in the order of $10^8 - 10^9$yr and is much shorter than the Hubble time

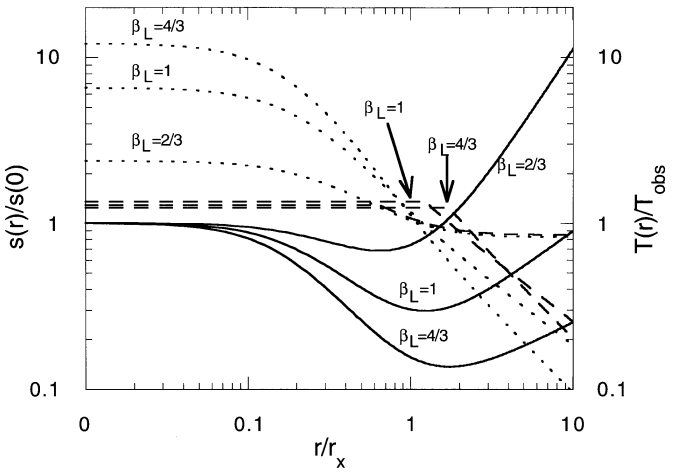

Fig. 5. Radial distributions of temperature and entropy in the case of the small core radius, $r_c = r_x/8$, for three different β_L. Short dashed lines show the temperature distribution defined in Sect. 2.2. Solid lines show the specific entropy distribution, $s(r) = P(r)/\rho_{gas}(r)^\gamma$, corresponding to these temperature distributions. Long dashed lines show the temperature distribution for isothermal core models defined in Sect. 6.1. Temperature distributions are normalized by the observed temperature, $T_{obs} = T_{em} \times T_c$, and entropy distributions are normalized by the central specific entropy.

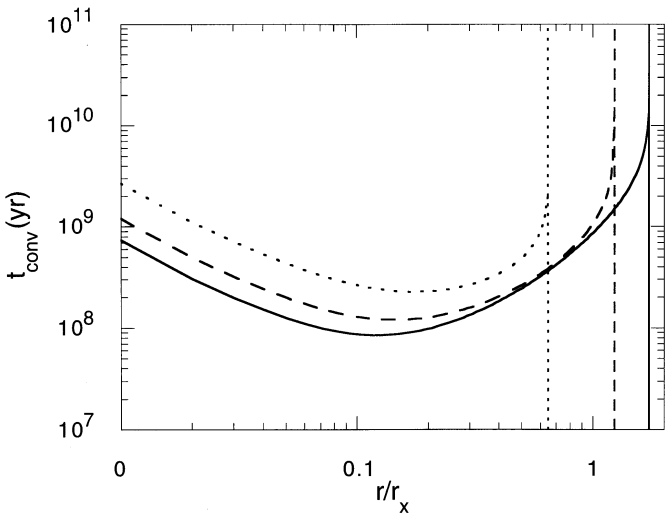

Fig. 6. Convective mixing time distribution for the same cluster mass distribution models as Fig. 5 and with T_x = 8keV. Short dashed line, long dashed line and solid line show the radial distributions of the convective mixing time for $\beta_L = 2/3,\ 1$ and $4/3$, respectively. Three vertical lines show the location of the marginally unstable point against the convective instability.

in almost all unstable regions. It is rather striking result that the gas density distribution like Coma cluster which has been though to be archetype of the gas density distribution of clusters for a long time, is unstable and can not maintain the structure no longer than 10% of the Hubble time.

In Figs. 2 and 3, the critical core radii for each β_L where the ICM distribution is marginally unstable against the convective instability are shown by three vertical lines. When the core radius of the cluster mass distribution is less than the critical value, a convectively unstable region appears in the central part of the ICM. These figures show that if the core radius of the mass distribution is more than two times less than that of X-ray core radius, there appears convectively unstable region in the central part of the ICM.

Now we speculate on the evolution of the ICM based on our results. One of our suggestion that the mass distribution in the sample clusters might have a large inhomogeneity implies the frequent occurrence of the cluster-cluster merging events at the medium redshift, say $z \sim 0.2 - 0.5$. Since the cluster-cluster merging might destroy cooling flow appeared in cluster central region due to shock heating (McGlynn & Fabian 1984, Schindler & Müller 1993), it implies that the cooling flows are frequently destroyed at the medium redshift. Once the cooling flow is destroyed, it is difficult to recover the cooling flow structure only by radiative energy loss since the cooling time exceeds the Hubble time, for example Coma cluster is though to have a recent merging event (Roettiger, Burns & Loken 1993) and the central cooling time is longer than the Hubble time. Therefore, the first suggestion might contradict with the fact that the high fraction, $\sim 70\%$, of nearby clusters have evidences of cooling flow (Edge, Stewart & Fabian 1991). However, the second suggestion of a high central mass concentration might provide one of the possible explanation for this contradiction. As shown above, the gas density distribution of non-cooling flow cluster is unstable against convective instability. Although the detailed study of the dynamical evolution of the merging clusters is required to know the detailed evolutional nature and the physical state of the final gas distribution, it suggests that the non-cooling flow type gas density distribution might approach to the centrally peaked gas density distribution, that is a convectively stable gas distribution, within $10^8 - 10^9$yr which is much less the Hubble time. Once the central gas density becomes high and the cooling time of the gas in the cluster central region becomes low due to the convective instability, cooling flow might be recovered. The quick recovering to the cooling flow due to the convective instability after the merging destruction of the cooling flow might explain the high fraction of nearby clusters having cooling flows if the cooling flows are destroyed frequently due to merging events at the medium redshift.

6. Non-thermal pressure supported models

6.1. An isothermal core model

The simple thermal pressure supported model discussed in the previous section could not be consistent with the observational data by Le Fèvre et al. One of the possibilities to reproduce the observed number of the giant luminous arcs is that X-ray temperature is not a good indicator of the gravitational potential depth of the cluster of galaxies, and non-thermal pressure plays an important role in supporting the gas against the gravitational pull, especially in the central region of the cluster (Miralda-

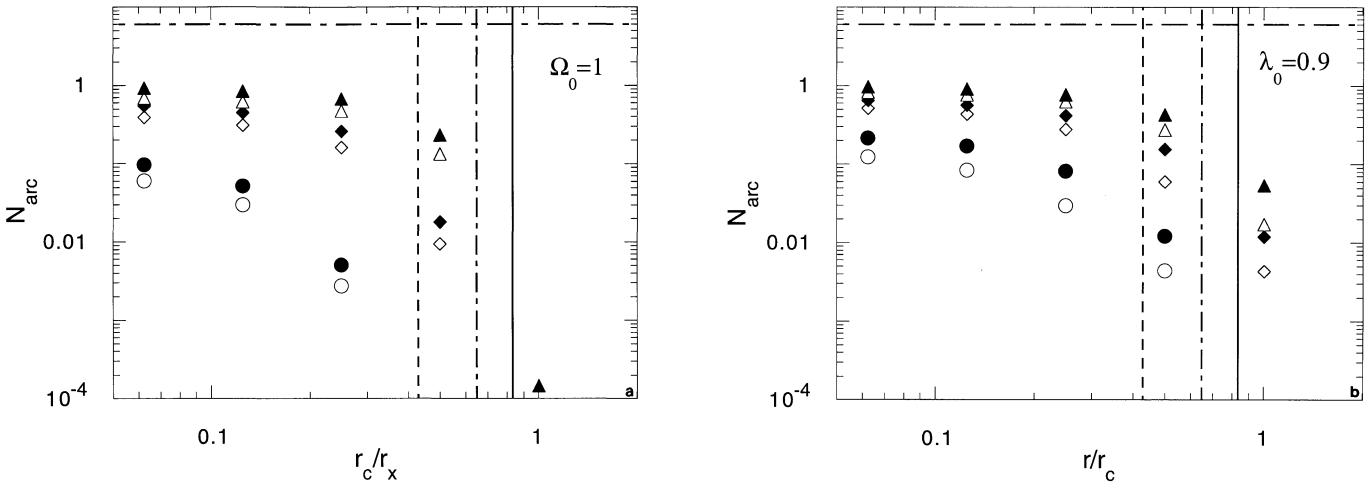

Fig. 7a and b. Predicted number of the giant luminous arcs in the isothermal core models with the detection conditions in **a** $(\Omega_0, \lambda_0, h) = (1.0, 0.0, 0.5)$ universe and **b** $(\Omega_0, \lambda_0, h) = (0.1, 0.9, 1.0)$ universe. Meaning of the symbols and lines are the same as those in Fig. 2.

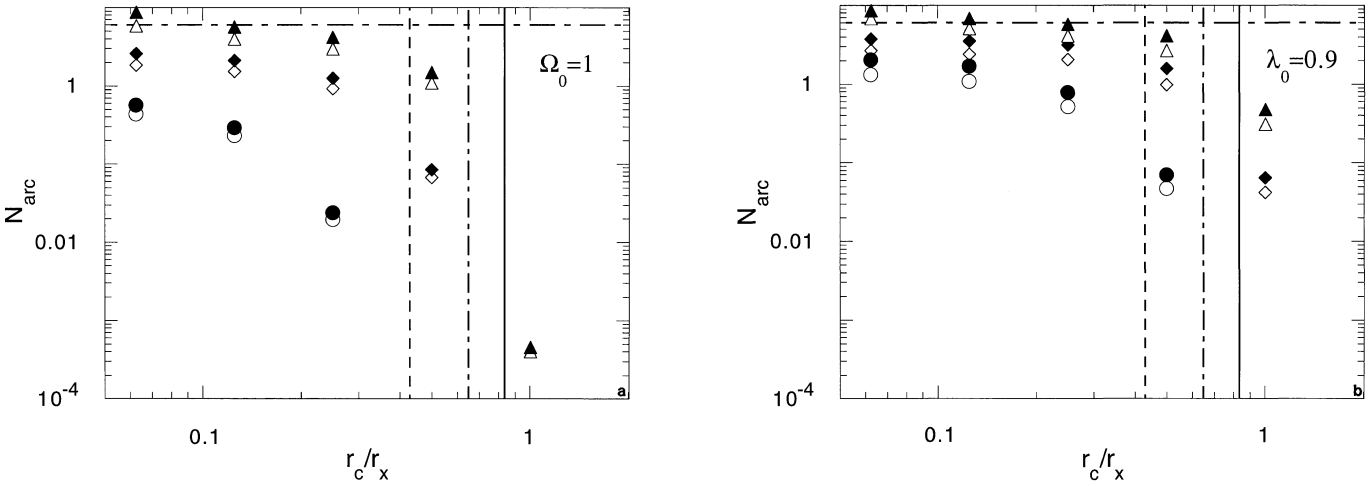

Fig. 8a and b. Predicted number of the giant luminous arcs in the isothermal core models without the detection conditions in (a) $(\Omega_0, \lambda_0, h) = (1.0, 0.0, 0.5)$ universe and (b) $(\Omega_0, \lambda_0, h) = (0.1, 0.9, 1.0)$ universe. Meaning of the symbols and lines are the same as those of Fig. 2.

Escudé & Babul 1995, Kneib et al. 1995, Loeb & Mao 1994). If the non-thermal pressure plays a significant role in cluster cores, an actual potential depth could be deeper than the estimations based on the purely thermal pressure supported model. This possibility could results in increase of the predicted number of the giant luminous arcs in Le Fèvre et al. sample. If dynamical pressure due to the random motion of the gas blobs (Kneib et al. 1995) is dominated against the thermal pressure, non-cooling flow type gas density distribution can be persisted longer than the convective mixing time even if the core radius of the mass distribution of cluster is much smaller than that of the ICM. In this section we will consider an extreme case of the possible modification of our model such that the expected number of giant luminous arcs will become much larger. There are several candidates as a source of the strong non-thermal pressure within the cluster core, namely magnetic pressure (Tribble 1993), dynamical pressure due to the random motion of the gas blobs (Kneib et al. 1995) and so on. However, we do not specify an origin of the non-thermal pressure here.

We have adopted the following model to quantify an effect of existence of the non-thermal pressure in the cluster core. By assuming the existence of the non-thermal isotropic pressure, the hydrostatic equation can be rewritten as

$$\frac{1}{\rho_{gas}(r)}\left[\frac{d\,P_{th}}{d\,r}+\frac{d\,P_{Nth}}{d\,r}\right]=-\frac{G\,M(r)}{r^2}, \qquad (25)$$

where P_{th} and P_{Nth} are thermal and non-thermal pressure, respectively, and $M(r)$ is the total mass contained within a sphere of the radius, r. By using specific thermal and non-thermal pressure, that is $\theta_{th} \equiv P_{th}/\rho_{gas}$ and $\theta_{Nth} \equiv P_{Nth}/\rho_{gas}$, the equa-

tion is reduced to

$$\frac{d\,(\theta_{th}(r)+\theta_{Nth}(r))}{d\,r}+(\theta_{th}(r)+\theta_{Nth}(r))\frac{1}{\rho_{gas}(r)}\frac{d\,\rho_{gas}(r)}{d\,r}=-\frac{G\,M(r)}{r^2}. \tag{26}$$

A solution for the total specific pressure, $\theta_{tot}(r) \equiv \theta_{th}(r) + \theta_{Nth}(r)$, is obtained in the similar form to Eq.(3), where χ is re-defined as $\chi = 4\pi G\rho_c r_c^2/\theta_{tot}(0)$. Since the behavior of the solution is exactly the same as Eq.(3), the solution with $\chi = \chi_{cr}$ is adopted in the following discussion.

Since most of non-cooling flow clusters of galaxies observed so far have an isothermal temperature distribution in the central region, we assume that the gas within the convectively unstable region is isothermal with the temperature at the marginally stable point and that the non-thermal pressure is zero in the convective stable region as one of the extreme models. Hereafter, we call this model isothermal core model. The distribution of the temperature in the isothermal core models is also shown in Fig. 5. The procedure to get the relation between the observed X-ray temperature and the cluster gravitational potential depth is the same as that explained in Sect. 2.2.

6.2. Arc statistics II: Isothermal core models

The isothermal core model predictions of number of the giant luminous arcs in the Le Fèvre et al. sample with and without the detection conditions are shown in Figs. 7 and 8, respectively. Although the predicted number increases a factor of 2 compared with the cases in the previous models, the predicted number with the detection conditions are, at least, 5 times less than the observed number. Therefore, the isothermal core models still cannot explain the results of Le Fèvre et al. arc survey.

6.3. Distribution of the source redshift and possibility of detecting distant galaxies in the forming era

None of our models examined so far could reproduce the observed large number of arcs found in Le Fèvre et al. sample. So we examine the redshift distribution of the source galaxies predicted by our models in order to see what happens. It illuminates how far we can observe through the cluster lenses and whether we can detect the distant forming galaxies through the cluster lenses.

In Fig. 9 we show the redshift distribution of the source galaxies for the isothermal core model with $\beta_L = 4/3$ and $r_c/r_x = 1/16$ for $(\Omega_0, \lambda_0, h) = (0.1, 0.9, 1.0)$ universe. This figure shows that the most of the giant luminous arcs are originated from spiral galaxies with the redshift less than 1. Contribution from the low redshift spheroidal galaxies is small. On the other hand, it also shows that there is a possibility to detect very high redshift spheroidal galaxies as giant luminous arcs. It is because the spheroidal galaxies in the formation epoch are very bright due to a high star formation rate. Thus if the SED of the UV bright elliptical NGC 4649 is a good representative of the spheroidal galaxies, the rate of detecting arcs becomes high as seen in Fig. 9b. Then we can expect to detect the spot of the galaxy formation in very high rate, namely a percentage of ten of the detected arcs. For comparison, Fig. 10 shows the redshift distribution of the source galaxies in the shallower gravitational potential models, namely ($\beta_L = 4/3$, $r_c/r_x = 1/2$) and ($\beta_L = 2/3$, $r_c/r_x = 1/16$). Since lensing is less effective, the predicted number of the giant luminous arcs decreases as shown in Fig. 7. Such decrease is significant for the giant luminous arcs originated from low redshift galaxies. Consequently the model increases the ratio of the number of arcs which are spheroidal galaxies nearly in their forming epoch to that of low redshift arcs.

7. Conclusions and discussion

We have constructed an arc identification scheme by consistently taking into account both of detection conditions in the arc survey and evolution of the source galaxies. We have then applied the scheme to arc statistics to constrain the cluster mass distribution models. The detection conditions decrease the number of detectable giant luminous arcs significantly by order of magnitude compared with the predicted number without the detection conditions. None of the presently assumed cluster mass distribution models can reproduce the large number of the giant luminous arcs as found in Le Fèvre et al.'s arc survey, and some of our basic assumption might be wrong. Irregularity and asymmetry in the cluster mass distribution could have significant effects on the arc statistics. For example, BSW have shown that the capability of their numerically modeled inhomogeneous clusters to produce giant luminous arcs is significantly higher than that of the non-singular isothermal sphere model with the same core radius and the same velocity dispersion as their model. However, we have shown that the expected number with BSW's model cluster is still order of magnitude less than the observed number and therefore their model cannot resolve the arc deficiency problem. We suggest that one of the remaining possibilities is that the mass concentration in the clusters is much more than that in BSW's numerically modeled clusters while they have inhomogeneity similar to BSW's model clusters as a whole. This gives an important speculation on the physical state and evolution of the hot gas in the cluster central region as discussed in Sect. 6. The gas density distribution in non-cooling flow clusters like Coma cluster which has been though to be archetype of the gas density distribution of clusters for a long time, might be unstable and is not able to maintain the structure no longer than 10% of the Hubble time. The quick recovering to the cooling flow due to the convective instability after the merging destruction of the cooling flow might explain the high fraction of nearby clusters having cooling flows even if the cooling flows are destroyed frequently due to merging events at the medium redshift. Redshift distribution of the source galaxies has been investigated. One of the striking results is that a comparatively large fraction of the source galaxies, approximately ten percent, have very high redshift. If the UV bright elliptical galaxy, NGC 4649, is a good representative of the majority of the spheroidal galaxies at high redshifts, these source galaxies

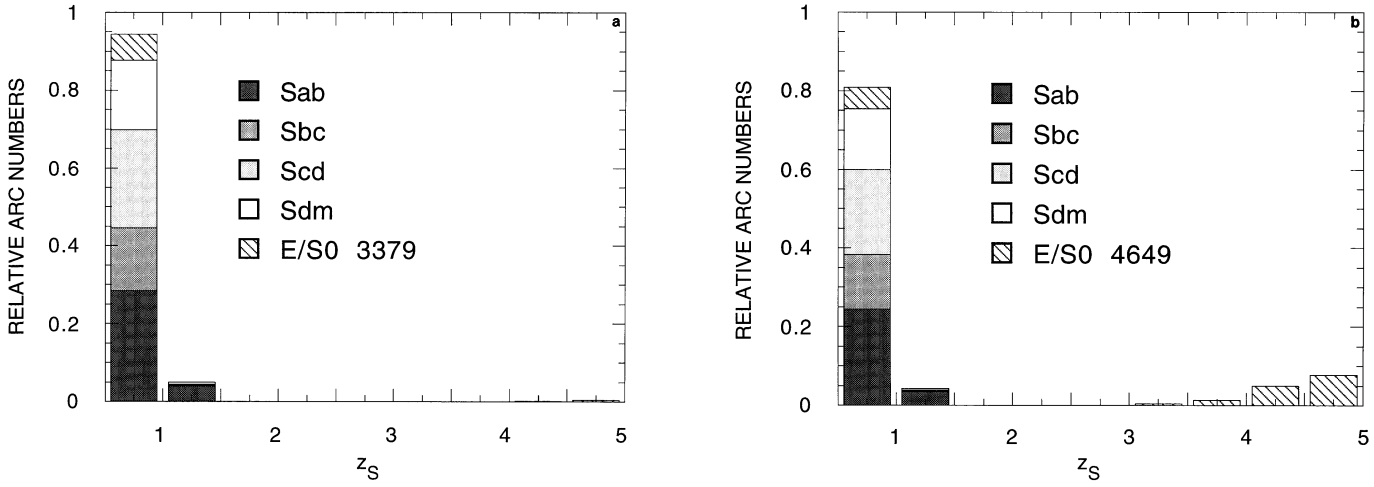

Fig. 9a and b. The redshift distribution of the relative number of the source galaxies of the giant luminous arcs in the isothermal core model with $\beta_L = 4/3$ and $r_c/r_x = 1/16$ with **a** NGC 3379 SED and with **b** NGC 4649 SED.

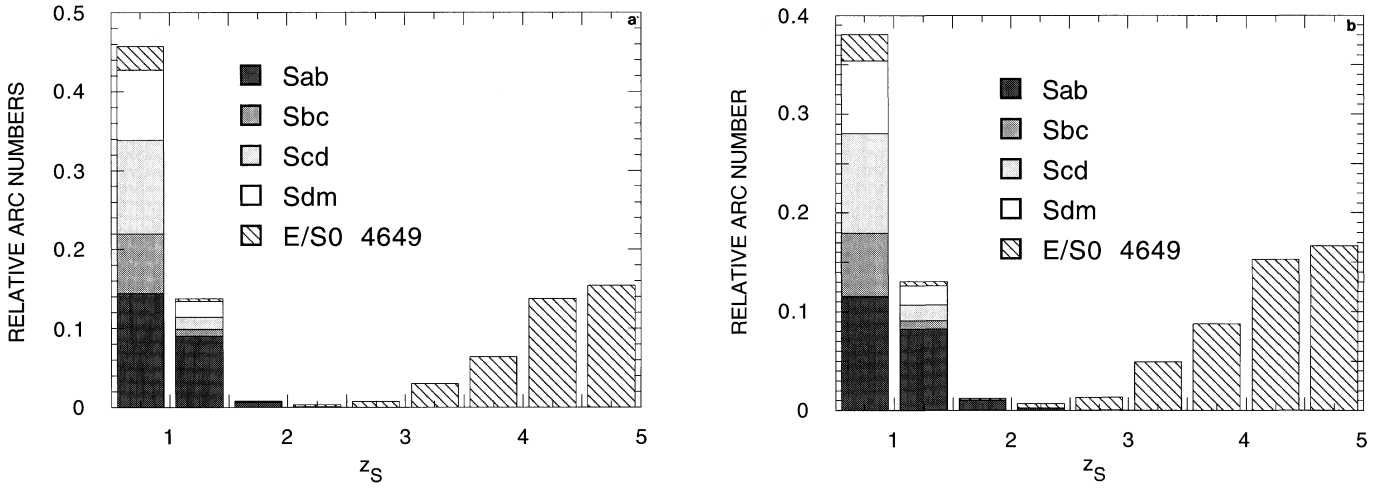

Fig. 10a and b. The redshift distribution of the relative number of the source galaxies of the giant luminous arcs in the shallower gravitational potential models than Fig. 9, namely **a** ($\beta_L = 4/3$, $r_c/r_x = 1/2$) and **b** ($\beta_L = 2/3$, $r_c/r_x = 1/16$). The results with NGC 4649 SED are shown.

might be in their forming era. Since we found that a simple thermal pressure supported model could not be consistent with the observational data by Le Fèvre et al., we have examined effects of the possibly existing non-thermal pressure at the center of cluster of galaxies as one of the possible extreme cases. However, we have numerically found that the modified lens model could not also explain the observed number by Le Fèvre et al.

Inclusion of the bulge components in spiral galaxies is one of the possibilities to resolve the arc deficiency problem since the bulge components are brighter than disk components at high redshifts. However, the expected increase of the number by taking into account the bulge components is, at most, a percentage of fifty. Let us suppose a half of the total luminosity of spiral galaxies is contributed by the bulge components. Since the proportion of the E/S0 is a percentage of twenty, the maximal effects of inclusion of the bulge components are estimated by artificially increasing the space density of E/S0 galaxies by a factor of five. According to the redshift distribution of the source galaxies for the model that predicts the largest number of the giant luminous arcs in the models examined here (see Fig. 9), contribution from E/S0 to the giant luminous arcs is at most ten percent. The expected increase of the number is then a factor of $1.4 (= 5 \times 0.1 + 0.9)$. The true increase should be less than 1.4 since the luminosity of the disk components becomes fainter by inclusion of the bulge components. Therefore, inclusion of the spiral bulge components cannot help large increase of the number.

Ambiguities in the X-ray data in the present analysis could also change the predicted number. We have extrapolated the empirical $T_x - L_x$ relation among nearby clusters to guess the temperature of the clusters in Le Fèvre et al. sample. Henry, Jiao & Gioia (1994) suggested that the $T_x - L_x$ relation for distant

clusters is different from that of the nearby clusters on the basis of the measurement of mean temperature of distant clusters. They showed that the temperature inferred from nearby $T_x - L_x$ relation is always higher than the measured mean temperature. If it is the case, true temperature of the clusters in Le Fèvre et al. sample should be lower than the presently used values, and the expected number becomes less further. Thus the discrepancy between model predictions and the observations becomes larger. Although their sample is limited, Tsuru et al. (1996) showed by measuring temperature of distant clusters using ASCA that the no evolution of $T_x - L_x$ relation is consistent within their sample distant clusters. In our analysis, the gas distribution in the clusters is modeled by a simple spherical β-model, and we have assumed that all of the sample clusters have the same gas distribution profile. This assumption could be good enough as the first approximation since X-ray luminosity of the all sample clusters is very similar to that of each other. However, we need temperature measurements by ASCA and precise measurement of the gas density distribution by ROSAT for all the clusters in Le Fèvre et al. sample in order to completely remove the model ambiguities.

Acknowledgements. The authors would like to thank Prof. Yoshii, Prof. Okamura and Dr. Miralda-Escudé for insightful comments. Especially, Dr. Miralda-Escudé gave us a lot of useful suggestions in order to improve the present work. KW would like to thank Prof. Hosoya and his colleagues for their hospitality and has been supported by JSPS Research Fellowships for Young Scientists. MH has been supported by the post doctoral program of MPE.

Appendix A

The basis of the gravitational lens theory has been discussed in many literatures (e.g., Refsdal 1964a, 1964b, Blandford & Narayan 1986), and its cosmological application, especially the Hubble parameter determination with gravitational lenses, was first discussed in the early work by Refsdal(1964b). Cosmological gravitational lens theory, especially a cosmological lens equation, has been formulated as Fermat's principle (e.g., Schneider 1985, Blandford & Narayan 1986). Sasaki(1993) reformulated the cosmological gravitational lens theory on the basis of the geodesic deviation equation (Ellis 1971) in an inhomogeneous (post-Newtonian) universe, and a role of the Dyer-Roeder distance (Dyer & Roeder 1972, 1973) in the cosmological lens equation was also clarified. The cosmological lens equation

$$\boldsymbol{\psi} = \boldsymbol{\theta} - \left(D_S^{(\tilde{\alpha})}/D_{LS}^{(\tilde{\alpha})}\right)\boldsymbol{\alpha}, \tag{A1}$$

where $\boldsymbol{\psi}$ and $\boldsymbol{\theta}$ are, respectively, angular position vectors of the source and the image, and $\boldsymbol{\alpha}$ denotes a deflection angle vector due to gravitational lensing. The distance factors are in the standard notations, and one has to use the generalized Dyer-Roeder distance with a smoothness parameter, $\tilde{\alpha}$, whose realistic value may be still unknown. The generalized Dyer-Roeder equation is

$$\begin{aligned}(1+z)\left[\Omega_0(1+z)^3 + (1-\Omega_0-\lambda_0)(1+z)^2 + \lambda_0\right]\frac{d^2D_A^{(\tilde{\alpha})}}{dz^2} \\ + \left[\frac{7}{2}\Omega_0(1+z)^3 + 3(1-\Omega_0-\lambda_0)(1+z)^2 + 2\lambda_0\right]\frac{dD_A^{(\tilde{\alpha})}}{dz} \\ + \frac{3}{2}\tilde{\alpha}\Omega_0(1+z)^2 D_A^{(\tilde{\alpha})} = 0.\end{aligned} \tag{A2}$$

Note that one has the usual angular diameter distance in the Friedmann model in the case, $\tilde{\alpha} = 1$.

Amplification and deformation factors of the gravitational lensed image are calculated in the following way. An image is represented by two Jacobi fields (e.g., Hawking & Ellis 1973), $Z^a_{(A)}\,(A = 1, 2)$, whose directions are the same as those of principal axes of the image. Assuming a circular source, deformation of the image is described by norms of the Jacobi fields. In our present interest, the thin lens approximation is appropriate, and any effects due to cosmic shear are negligibly small (Futamase & Sasaki 1989, Watanabe & Sasaki 1990). Under these assumptions, one can show, with the null geodesic deviation equation, that quantitative measure of the image deformation is given by ratio of one eigen value, M_x, to another eigen value, M_y, of the Jacobi matrix, $\partial\boldsymbol{\psi}/\partial\boldsymbol{\theta}$. Image deformation rates along minor and major axes are then given by, respectively,

$$A_1 = 1/\max\left(|M_x|, |M_y|\right), \quad A_2 = 1/\min\left(|M_x|, |M_y|\right), \tag{A3}$$

and an amplification factor and an axis ratio of the image are given by $A = A_1A_2$ and $\epsilon = A_2/A_1$, respectively

The lens equation and basic quantities, M_x and M_y, in our lens model are easily calculated, and we summarize them below, where we use the notations, $\boldsymbol{b}_0 = \boldsymbol{\theta}D_L^{(\tilde{\alpha})}/r_{\rm c}$, $\boldsymbol{\ell}_0 = \boldsymbol{\psi}D_L^{(\tilde{\alpha})}/r_{\rm c}$, and $R_0 = R/r_{\rm c}$, which are similar to those in Wu & Hammer (1993).

(1) $\beta_{\rm L} = 2/3$

$$\begin{aligned}\boldsymbol{\ell}_0 =& \boldsymbol{b}_0[1 - \frac{4D}{\pi b_0^2}\left\{R_0 - \sqrt{R_0^2 - b_0^2}\right. \\ &\left. + \sqrt{1+b_0^2}\tan^{-1}\sqrt{\frac{R_0^2-b_0^2}{1+b_0^2}} - \tan^{-1}R_0\right\}], \\ M_x =& 1 - \frac{4D}{\pi b_0^2}\left\{R_0 - \sqrt{R_0^2 - b_0^2}\right. \\ &\left. + \sqrt{1+b_0^2}\tan^{-1}\sqrt{\frac{R_0^2-b_0^2}{1+b_0^2}} - \tan^{-1}R_0\right\}, \\ M_y =& 1 + \frac{4D}{\pi b_0^2}\left\{R_0 - \sqrt{R_0^2 - b_0^2}\right. \\ &\left. + \frac{1}{\sqrt{1+b_0^2}}\tan^{-1}\times\sqrt{\frac{R_0^2-b_0^2}{1+b_0^2}} - \tan^{-1}R_0\right\}, \\ D =& 4\pi^2 G\rho_{\rm c}r_{\rm c}^2\left(\frac{D_L^{(\tilde{\alpha})}D_{LS}^{(\tilde{\alpha})}}{r_{\rm c}D_S^{(\tilde{\alpha})}}\right).\end{aligned} \tag{A4}$$

(2) $\beta_{\rm L} = 1$

$$
\begin{aligned}
\boldsymbol{\ell}_0 =& \boldsymbol{b}_0[1 - \frac{2D}{b_0^2}\left\{\sqrt{\frac{R_0^2 - b_0^2}{1+R_0^2}} - \frac{R_0}{\sqrt{1+R_0^2}}\right. \\
&\left. + \ln\left[\frac{(R_0+\sqrt{1+R_0^2})\sqrt{1+b_0^2}}{\sqrt{R_0^2-b_0^2}+\sqrt{1+R_0^2}}\right]\right\}], \\
M_x =& 1 - \frac{2D}{b_0^2}\left\{\sqrt{\frac{R_0^2 - b_0^2}{1+R_0^2}} - \frac{R_0}{\sqrt{1+R_0^2}}\right. \\
&\left. + \ln\left[\frac{(R_0+\sqrt{1+R_0^2})\sqrt{1+b_0^2}}{\sqrt{R_0^2-b_0^2}+\sqrt{1+R_0^2}}\right]\right\}, \\
M_y =& 1 + \frac{2D}{b_0^2}\left\{\frac{1}{\sqrt{1+R_0^2}}\left(\frac{R_0^2}{\sqrt{R_0^2-b_0^2}} - R_0\right)\right. \\
&\left. - \frac{b_0^2}{1+b_0^2}\sqrt{\frac{1+R_0^2}{R_0^2-b_0^2}} + \ln\left[\frac{(R_0+\sqrt{1+R_0^2})\sqrt{1+b_0^2}}{\sqrt{R_0^2-b_0^2}+\sqrt{1+R_0^2}}\right]\right\}, \\
D =& 8\pi G\rho_{\rm c} r_{\rm c}^2\left(\frac{D_L^{(\tilde{\alpha})} D_{LS}^{(\tilde{\alpha})}}{r_{\rm c} D_S^{(\tilde{\alpha})}}\right).
\end{aligned}
\tag{A5}
$$

(3) $\beta_{\rm L} = 4/3$

$$
\begin{aligned}
\boldsymbol{\ell}_0 =& \boldsymbol{b}_0[1 - \frac{4D}{\pi b_0^2}\left\{\frac{1}{1+R_0^2}\left(\sqrt{R_0^2-b_0^2} - R_0\right)\right. \\
&\left. - \frac{1}{\sqrt{1+b_0^2}}\tan^{-1}\sqrt{\frac{R_0^2-b_0^2}{1+b_0^2}} + \tan^{-1}R_0\right\}], \\
M_x =& 1 - \frac{4D}{\pi b_0^2}\left\{\frac{1}{1+R_0^2}\left(\sqrt{R_0^2-b_0^2} - R_0\right)\right. \\
&\left. - \frac{1}{\sqrt{1+b_0^2}}\tan^{-1}\sqrt{\frac{R_0^2-b_0^2}{1+b_0^2}} + \tan^{-1}R_0\right\}, \\
M_y =& 1 + \frac{4D}{\pi b_0^2}\left\{\frac{1}{1+R_0^2}\left(\frac{\sqrt{R_0^2-b_0^2}}{1+b_0^2} - R_0\right)\right. \\
&\left. - \frac{1+2b_0^2}{\left(1+b_0^2\right)^{3/2}}\tan^{-1}\sqrt{\frac{R_0^2-b_0^2}{1+b_0^2}} + \tan^{-1}R_0\right\}, \\
D =& 2\pi^2 G\rho_{\rm c} r_{\rm c}^2\left(\frac{D_L^{(\tilde{\alpha})} D_{LS}^{(\tilde{\alpha})}}{r_{\rm c} D_S^{(\tilde{\alpha})}}\right).
\end{aligned}
\tag{A6}
$$

A lensing parameter, D, is defined such that its critical value is 1 in the limit of $R_0 \to \infty$. Therefore, the lensing parameter, D, can be interpreted as an effective surface mass density of the cluster of galaxies in the unit of the critical surface mass density (Blandford & Narayan 1986). We numerically found that, when $D < 1$, $\epsilon < 3$ for any values of b_0 and R_0, that the arc forming region on the source plane consists, at most, of two disconnected regions, and that the number of arcs is, at most, three.

References

Arimoto,N., Yoshii,Y. 1986, A&A **164**, 260.
——. 1987, A&A **173**, 23.
Bartelmann,M. 1995, A&A **299**, 11.
Bartelmann,M., Weiss,A. 1994, A&A **287**, 1.
Bartelmann,M., Steinmetz,M., Weiss,A. 1995, A&A **297**, 1 (BSW).
Binggeli,B., Tarenghi,M., Sandage,A. 1990, A&A **228**, 42.
Blandford, R.D., Narayan, R. 1986, ApJ **310**, 568.
Bonnet,H., Mellier,Y., Fort,B. 1994, ApJ, **427**, L83.
Briel,U.G., Henry,J.P., Schwarz,R.A., Böhringer,H., Ebeling,H., Edge,A.C., Hartner,G.D., Schindler,S., Trümper,J., Voges,W. 1991, A&A **246**, L10.
Briel,U.G., Henry,J.P., Böhringer,H. 1992, A&A **259**, L31.
Bruzual,A.G., Kron,R.G. 1980, ApJ **241**, 25.
Bruzual,A.G. 1983, ApJ **273**, 105.
Carlberg,R.G., Yee,H.K.C., Ellingson,E. 1994, ApJ **437**, 63.
Crampton,D., Morbey,C.L., Le Fèvre,O., Hammer,F., Tresse,L., Lilly,S.J., Schade,D.J. 1994, SISSA preprint.
David,L.P., Slyz,A., Jones,C., Forman,W., Vrtilek,S.D., Arnaud,K.A. 1993, ApJ **412**, 479.
Defouw,R.J. 1970, ApJ **160**, 659.
de Vaucouleurs,G. 1962, in IAU Symp. 15, Problems of Extragalactic Research, MacVittie,G.C. (ed.), (MacMillan, New York) p.3.
Donahue,M.E.,Stocke,J.T., Gioia,I.M. 1992, ApJ **385**, 49.
Dyer, C.C., Roeder, R.C. 1972, ApJ **174**, L115.
——. 1973, ApJ 180, L31.
Edge, A.C., Stewart, G.C., Fabian, A.C. 1992, MNRAS **258**, 177.
Efstathiou,G., Ellis,R.S., Peterson,B.A. 1988, MNRAS **232**, 431.
Ellis, G.F.R. 1971, General relativity and cosmology, ed. Sachs, B.K. (Academic Press, New York), p.104.
Fabian,A.C. 1994, ARA&A **32**, 277.
Fahlman,G.G., Kaiser,N., Squires,G.,Woods,D. 1994, ApJ **437**, 56.
Fort,B., Mellier,Y. 1994, A&AR **5** 239.
Freeman,K.C. 1970, ApJ **160**, 811.
Fukugita,M., Takahara,F., Yamashita,K., Yoshii,Y. 1990, ApJ **361**, L1.
Futamase, T., Sasaki, M. 1989, Phys. Rev. **D40**, 2502.
Griffiths,R.E. et al. 1994, ApJ **435**, L19.
Hattori,M., Yoshida,T., Habe,A. 1995, MNRAS **275**, 1195.
Hawking, S.W., Ellis, G.F.R. 1973, The large scale structure of space-time, (Cambridge University Press, Cambridge) p.96.
Heisler,J., Ostriker,J.P. 1988, ApJ **332**, 543.
Henry,J.P., Jiao,L., Gioia,I.M. 1994, ApJ **432**, 49.
Hughes,J.P. 1989, ApJ **337**, 21.
James,P.J., Puxley, P.J. 1993, Nature **363**, 240.
Jones,C., Forman,W. 1990, in Clusters of Galaxies, Oegerle,W., Fitchett,M.J., Danly,L. (eds.), (Cambridge Univ. Press, Cambridge) p.257.
Kaiser,N., Squires,G. 1993, ApJ **404**, 441.
Kaiser,N., Squires,G., Fahlman,G.G., Woods,D., Broadhurst,T. 1994 preprint.
Kneib,J.P., Mellier,Y., Pelló,R., Miralda-Escudé,J., Le Borgne,J.-F., Böhringer,H., Picat,J.-P. 1995, AA **303**, 27.
Kochanek,C.S. 1990, MNRAS **247**, 135.
Le Fèvre,O., Hammer,F., Angonin,M.C., Gioia,I.M., Luppino,G.A. 1994, ApJ **422**, L5.
Loeb,A., Mao,S. 1994, ApJ **435**, L109.
Lubin,L.M., Bahcall,N.A. 1993, ApJ **415**, L17.
Lynds,R., Petrosian,V. 1986, BAAS **18**, 1014.
McGlynn,T.A., Fabian,A.C. 1984, MNRAS **208**, 709.
Miralda-Escudé,J. 1991, ApJ **370**, 1.

Miralda-Escudé,J. 1993a, ApJ **403**, 497.
Miralda-Escudé,J. 1993b, ApJ **403**, 509.
Miralda-Escudé,J., Babul,A. 1995, ApJ **449**, 18.
Nemiroff,R.J., Dekel,A. 1989, ApJ **344**, 51.
Pence,W. 1976, ApJ **203**, 39.
Refsdal, S. 1964a, MNRAS **128**, 307.
——. 1964b, MNRAS **128**, 315.
Roettiger,K., Burns,J., Loken,C. 1993, **407**, L53.
Sasaki, M. 1993, Prog. Theor. Phys. **90**, 753.
Schindler,S., Müller,E. 1993, A&A **272**, 137.
Schindler,S., Guzzo,L., Ebeling,H., Böhringer,H., Chincarini,G., Collins,C.,A., De Grandi,S., Neumann,D.,M., Briel,U.,G., Shaver,P.,A., Vettolani,G. 1995, **299**, L9.
Schindler,S., Hattori,M., Neumann,D.,M., Böhringer,H. 1996 submitted to A&A.
Schneider,P. 1985, A&A **143**, 413.
Schneider,P. 1995, A&A **302**, 9.
Schneider,P., Seitz,C. 1995, A&A **294**, 411.
Seitz,C., Schneider,P. 1995, A&A **297**, 287.
Smail,I., Ellis,R.S., Fitchett,M.J., Edge,A.C. 1995, MNRAS **273**, 277.
Soucail,G., Fort,B., Mellier,Y., Picat,J.P. 1987, A&A **172**, L14.
Soucail,G., Mellier,Y., Fort,B., Mathez,G., Cailloux,M. 1988, A&A **191**, L19.
Squires,G., Kaiser,N., Babul,A., Fahlamn,G., Woods,D., Neumann,D.M., Böhringer,H. 1995, submitted to ApJ.
Tribble,P.C. 1993, MNRAS **263**, 31.
Tsuru,T., Koyama,K., Hughes,J.,P., Arimoto,N., Kii,T., Hattori,M. 1996, in *The 11th international colloquium on UV and X-ray spectroscopy of Astrophysical and Laboratory Plasma* (eds. Watanabe,T., Yamashita,K.) in press.
Tyson,J.A. 1988, AJ **96**, 1.
Tyson,J.A., Valdes,F., Wenk,R.A. 1990, ApJ **349**, L1.
Watanabe, K., Sasaki, M. 1990, PASJ **42**, L33.
Waxman,E., Miralda-Escudé,J. 1995 ApJ in press.
Webster,R.L. 1985 MNRAS **213**, 871.
Wu, X.-P., Hammer,F. 1993 MNRAS **262**, 187.
Wu, X.-P. 1994, ApJ **436**, L115.
Yoshii,Y., Takahara,F. 1988, ApJ **326**, 1.
Yoshii,Y., Peterson,B.A. 1991, ApJ **372**, 8.
Yoshii,Y. 1993, ApJ **403**, 552.

This article was processed by the author using Springer-Verlag LaTeX A&A style file *L-AA* version 3.